Int. J. Solids Structures Vol. 21, No. 12, pp. 1149–1163, 1985
Printed in Great Britain.

0020–7683/85 $3.00 + .00

A CLASS OF PLASTIC CONSTITUTIVE EQUATIONS WITH VERTEX EFFECT—IV. APPLICATIONS TO PREDICTION OF FORMING LIMIT STRAINS OF METAL SHEETS UNDER NONPROPORTIONAL LOADINGS

MANABU GOTOH
Department of Precision Engineering, Gifu University, Yanagido 1-1, Gifu-City, 501-11, Japan

(*Received* 20 *November* 1983)

Abstract—The new plastic (elastoplastic) constitutive equation with vertex effect which was proposed and developed in the previous papers is applied to prediction of the forming limit strains of metal sheets which are subjected to various nonproportional loading without unloading and to proportional loading after another proportional loading with or without unloading. It is demonstrated that the constitutive equation is very effective, that appropriately curved strain-paths give much larger limiting strains than the corresponding straight paths do, that abrupt change in stress- or strain-path very often induces a catastrophic breakage at the instant of the path-change, and that very useful secondary FLDs (forming limit diagrams) can be drawn.

INTRODUCTION

In Parts I and II of this series of work[1, 2], a new type of plastic constitutive equations with vertex effect and its extension to more general inelastic constitutive equations were proposed, and discussions on them were presented. And in Part III[3], its simplest form was applied to calculation of FLDs (forming limit diagrams) of metal sheets subjected to proportional loadings.

In this paper the same type of constitutive equation as that used in Part III is applied to predict forming limit strains of metal sheets which are deformed along arbitrarily curved strain-paths without unloading, and deformed along straight strain-path after another straight strain-path, with or without unloading at the strain-path change. The localized bifurcation condition due to Stören and Rice[4] is used as the breakage condition of the sheets. Chu[5] presented discussions similar to some portion of ours on the base of J_2-corner theory due to Christoffersen and Hutchinson[6]. Here our attention is payed on far more extensive strain-paths in order to obtain more positive and practical informations on the forming limit strains of the metal sheets, and to confirm the effectiveness of our plastic constitutive equation on the subject.

2. BASIC EQUATIONS

The constitutive equation used here is written as follows[1–3]:

$$\mathrm{d}\mathbf{e} = \mathrm{d}\mathbf{e}^e + \mathrm{d}\mathbf{e}^p = (1/2G^*)\,\mathring{\mathrm{d}}\mathbf{T} + \langle P(\Theta)\rangle(b/2\bar{\sigma}h_0)\mathbf{T}\,\overline{\mathrm{d}\sigma}, \tag{1}$$

where

$$\begin{aligned}
\mathrm{d}\mathbf{e} &= \mathrm{d}\boldsymbol{\epsilon} - (1/3)(\mathrm{tr}\,\mathrm{d}\boldsymbol{\epsilon})\mathbf{1},\\
1/G^* &= 1/G + \langle P\rangle/H_0,\\
\mathbf{T} &= \boldsymbol{\sigma} - (1/3)(\mathrm{tr}\,\boldsymbol{\sigma})\mathbf{1},\\
\mathring{\mathrm{d}}\mathbf{T} &= \mathrm{d}\mathbf{T} - \mathrm{d}\boldsymbol{\omega}\mathbf{T} + \mathbf{T}\,\mathrm{d}\boldsymbol{\omega},\\
\bar{\sigma} &= \sqrt{3/2}(\mathrm{tr}\,\mathbf{T}^2)^{1/2},\\
\overline{\mathrm{d}\sigma} &= \sqrt{3/2}(\mathrm{tr}\,\mathring{\mathrm{d}}\mathbf{T}^2)^{1/2} \neq \mathrm{d}\bar{\sigma},\\
h_0 &= (1/3)\,\overline{\mathrm{d}\sigma}/\overline{\mathrm{d}\epsilon^p} \text{ for proportional loading},\\
\overline{\mathrm{d}\epsilon^p} &= \sqrt{2/3}(\mathrm{tr}\,\mathrm{d}\boldsymbol{\epsilon}^{p2})^{1/2},
\end{aligned}$$

and $d\boldsymbol{\epsilon}$ = strain increment, $\boldsymbol{\sigma}$ = Cauchy stress, and the superfixes e and p denote elasticity and plasticity, respectively. And $\mathbf{1}$ = unity tensor of second rank, G = elastic shear rigidity modulus, and the symbol tr denotes the trace operator. $d\boldsymbol{\omega}$ = increment of rigid-body rotation. h_0 and H_0 denote the instantaneous work-hardening rate and the instantaneous vertex-hardening rate for proportional loading, respectively. And,

$$\begin{aligned} b &= 1 - a, \\ P(\Theta) &= a + b \cos \Theta, \\ \langle P \rangle &= P \qquad \text{for } P > 0, \\ &= 0 \text{ for } P \leqq 0, \\ a &= h_0/H_0 = \cos \Theta_0/(1 + \cos \Theta_0), \end{aligned}$$

where the angle Θ denotes that between $\mathbf{T}$ and $\mathring{d}\mathbf{T}$ in the five-dimensional deviatoric stress space due to Illushin[7], and is defined by the following relation:

$$\cos \Theta = \operatorname{tr}(\mathbf{T}\,\mathring{d}\mathbf{T})/[(\operatorname{tr}\mathbf{T}^2)(\operatorname{tr}\mathring{d}\mathbf{T}^2)]^{1/2}.$$

Here we assume plastic deformation to be incompressible. Then we have the following relation between the increments of volume-strain and hydrostatic stress:

$$\operatorname{tr} d\boldsymbol{\epsilon} = (1/3K)(\operatorname{tr} d\boldsymbol{\sigma}), \tag{2}$$

where K = elastic bulk modulus.

One of the characteristic aspects of the constitutive equation (1) is that it allows a pointed vertex to evolve at the loading point on the subsequent loading surface as far as H_0 remains finite, and at this point it is essentially different from the classical plastic potential theory. In this case, it is natural to think that the vertex will develop with plastic deformation, for the initial yield surface should be considered to be generally smooth at the initial yield point for arbitrary loading. (Note that even for a Tresca material the yield surface is smooth except at particular points on it.) The angle Θ_0 in eqn (1) denotes the half angle of the point-wise vertexed loading surface cone in the five-dimensional deviatoric stress space. Therefore, it can be formulated most simply as follows:

$$\Theta_0 = \pi/2 - \rho\epsilon^2, \qquad \epsilon = \int \overline{d\epsilon^p}, \tag{3}$$

where ρ is the newly introduced material constant which governs the rate of evolution of the pointed vertex. If ρ always remains equal to 0 with plastic deformation, then no vertex forms on the loading surface and the constitutive equation (1) reduces to the classical J_2-flow theory, which corresponds to the case where H_0 always remains infinite.

Another characteristic aspect of our constitutive equation (1) is that it uses not only the usual strain-history measure $\overline{d\epsilon}$ which is defined as

$$\overline{d\epsilon} = \sqrt{2/3}(\operatorname{tr} d\mathbf{e}^2)^{1/2},$$

but also the stress-history measure $\overline{d\sigma}$ defined above which is different from the increment of Mises equivalent stress $\bar{\sigma}$ which is written as follows:

$$d\bar{\sigma} = (3/2\bar{\sigma})\operatorname{tr}(\mathbf{T}\,\mathring{d}\mathbf{T}).$$

As discussed in Part I, the function $P(\Theta)$ can be rather easily formulated by virtue of the introduction of $\overline{d\sigma}$ and is described above. Moreover, our constitutive equation (1)

can be easily extended to more general types of inelasticity, or to that for the case where arbitrary initial and subsequent anisotropy plays an important role (see Part I). These aspects are totally different from J_2-corner theory due to Christoffersen and Hutchinson[6].

The expression (1) is convenient for the case where the stress-path is controlled. The inverse expression of it is needed for the case where the strain-path is controlled, and is written as follows:

$$\begin{aligned} \mathring{\mathrm{d}}\mathbf{T} &= 2G^*[\mathbf{de} - \langle P\rangle(3b/2\bar{\sigma})(\bar{h}/h_0)\mathbf{T}\,\overline{\mathrm{d}\epsilon}], \\ \bar{h}/h_0 &= [C_1^2 + 2C_1C_2\cos\Theta + C_2^2]^{-1/2}, \\ C_1 &= \gamma + a\langle P\rangle, \qquad \gamma = h_0/G, \qquad C_2 = b\langle P\rangle. \end{aligned} \tag{4}$$

When the strain-path is controlled, $\mathbf{de}$ and $\overline{\mathrm{d}\epsilon}$ are given and thus the angle θ between $\mathbf{de}$ and $\mathbf{T}$ is also known, where

$$\cos\theta = \mathrm{tr}(\mathbf{T}\,\mathbf{de})/[(\mathrm{tr}\,\mathbf{T}^2)(\mathrm{tr}\,\mathbf{de}^2)]^{1/2}.$$

And we have the following relation between $\cos\theta$ and $\cos\Theta$:

$$\cos\theta = (C_1\cos\Theta + C_2)/[C_1^2 + 2C_1C_2\cos\Theta + C_2^2]^{1/2}. \tag{5}$$

This can be rather easily solved with respect to $\cos\Theta$ by a direct numerical method. [Or, as described in the Part II, if nonproportionality of the strain-path is not very severe in a numerical analysis of large deformation by incremental method (say), we may use the value of $\cos\Theta$ at one step earlier as its good approximation without solving eqn (5) at every step of deformation, although in all the numerical examples given below, the direct solution of eqn (5) is used in order to keep good accuracy of calculation.]

The condition for continuity of plastic deformation for next $\mathring{\mathrm{d}}\mathbf{T}$ in the expression (1) is given as

$$0 \leqq \Theta < \Theta_{\max},$$

and that for next $\mathbf{de}$ in the expression (4) is given as

$$0 \leqq \theta < \Theta_{\max},$$

where

$$\Theta_{\max} = \cos^{-1}(-a/b) \geqq \pi/2,$$

$$\Theta_0 = \pi - \Theta_{\max}.$$

Here we concern ourselves with thin sheets. Therefore the constitutive equation (1) or (4) is reduced to its special form of plane stress state, though its detail is omitted here.

Now let us consider an element of thin sheet (see Fig. 1). In Fig. 1, σ_1 is the major

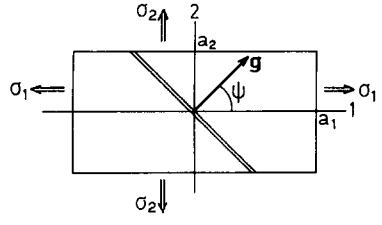

Fig. 1. A thin sheet element under biaxial loading.

principal stress and is assumed to be positive. As for the total principal strains ϵ_1 and ϵ_2, we consider deformation within the range of $|\epsilon_1| \geqq |\epsilon_2|$ and $\epsilon_1 > 0$. The dimension of the length of the sides a_1 and a_2 may be arbitrary, and this element can be thought to be either a macroscopic thin plate undergoing uniform deformation or a small element within a large thin sheet undergoing not very severely nonuniform deformation. Of course, in the latter case, the dimension of the element should be large enough to use the assumption of plane stress state.

Therefore the element is assumed to deform with straight sides due to some constraint, and thus the state of stress and strain is uniform until a localized neck band (a kind of bifurcation of local type which was first discussed in detail and used as a breakage condition by Stören and Rice[4]) takes place, as illustrated in Fig. 1, and the sheet breaks. [Of course, for symmetry, two such bands in a cross manner could form at the same time, though one of them usually predominates because of very slight heterogeneity of the actual material property.] As is well known, a localized necking is accompanied with very severe thinning within a very localized area of narrow band whose width is comparable to the thickness of the sheet. Thus the condition of the onset of this type of bifurcation is justified to use as the condition of breakage of the thin sheet undergoing uniform deformation or of breakage at a point on a large-scale thin sheet undergoing not very severely nonuniform deformation. For this reason, check of the onset of another type of bifurcation (the so-called diffuse necking) is omitted here, because our attention is payed exclusively to breakage phenomenon of the sheet.

Let us consider the instant at which an incipient localized neck band has appeared, as illustrated in Fig. 1. It is the band along which discontinuities in distributions of stress-increment and of gradient of displacement-increment exist, and whose width is comparable with the sheet thickness. Then, following the similar procedure used in the previous Part III by use of our constitutive equation, the equilibrium equation across the band and so forth, we obtain the following fourth-order algebraic equation with respect to g_1 and g_2, where the vector $\mathbf{g}(g_1, g_2)$ represents the unit normal to the band. Here, for simplicity, we keep τ_{12} and $\mathring{\tau}_{12}$ equal to 0 outside of the band, both of which are externally controlled:

$$Ag_1^4 + Cg_1^2g_2^2 + Eg_2^4 = 0, \tag{6}$$

$$A = (a_{11} - \sigma_1)(a_{33} + \hat{\tau}), \qquad E = (a_{22} - \sigma_2)(a_{33} - \hat{\tau}),$$

$$C = (a_{11} - \sigma_1)(a_{22} - \sigma_2) + a_{33}^2 - \hat{\tau}^2 - (a_{12} + a_{33} - \hat{\sigma})(a_{21} + a_{33} - \hat{\sigma}),$$

$$\hat{\sigma} = (\sigma_1 + \sigma_2)/2, \qquad \hat{\tau} = (\sigma_1 - \sigma_2)/2.$$

These are formally similar to the corresponding equations in Part III. However, the coefficients $a_{11} \sim a_{33}$ are dependent not only on the stress ratio $m = \sigma_2/\sigma_1$ and the strain ratio $\alpha = \epsilon_2/\epsilon_1$, but also on the stress-increment ratio $m' = \mathring{d}\sigma_2/\mathring{d}\sigma_1$ or the strain-increment ratio $\alpha' = d\epsilon_2/d\epsilon_1$, all of which have to be estimated at every step of incremental calculation, because here we concern ourselves with arbitrarily nonproportional deformation. They are expressed by the following equations:

$$a_{11} = (1/D^*)[(1/3G^*) + (1/12h_0)(bm_1/M)^2 + (\kappa/12h_0)ab(4m'm_1 + m_3)/(MM')],$$

$$a_{22} = (1/D^*)[(1/3G^*) + (1/12h_0)(bm_2/M)^2 + (\kappa/12h_0)ab(4m_1 + m'm_4)/(MM')],$$

$$a_{12} = (1/D^*)[(1/6G^*) - (1/12h_0)m_1m_2(b/M)^2 + (\kappa/12h_0)ab(2m'm_1 - m_4)/(MM')],$$

$$a_{21} = (1/D^*)[(1/6G^*) - (1/12h_0)m_2m_1(b/M)^2 + (\kappa/12h_0)ab(2m_2 - m'm_3)/(MM')],$$

$$a_{33} = 1/[(1/G^*) + (\kappa/2h_0)ab(m_2 + m'm_1)/(MM')],$$

$$D^* = (1/12)[(1/G^*)^2 + (1/h_0G^*)b^2] + (Mab/4M'h_0)[(1/G^*) + (b^2/3h_0)]$$
$$+ (1/6h_0^2)(Mab/M')^2,$$

where

$$1/G^* = (1/G) + (a/H_0), \quad m_1 = 2m - 1, \quad m_2 = 2 - m,$$
$$m_3 = 5 - 4m, \quad m_4 = 5m - 4, \quad \kappa = (\text{sign of } \mathring{\sigma}_{11}), \quad M = (1 - m + m^2)^{1/2},$$
$$M' = (1 - m' + m'^2)^{1/2}.$$

[If τ_{12} and $\mathring{\tau}_{12}$ are not equal to 0 at the time under consideration, the equation corresponding to eqn (6) takes the following form:

$$Ag_1^4 + Bg_1^3 g_2 + Cg_1^2 g_2^2 + Dg_1 g_2^3 + Eg_2^4 = 0, \tag{7}$$

and the coefficients $A \sim E$ take more complex expressions.]

In the eqns (6) and (7), the characteristics of material work-hardening has its effect through h_0, and therefore both of them are valid, irrespective of the type of work-hardening. For example, when the work-hardening property is expressed by the following equation

$$\bar{\sigma} = c\dot{\bar{\epsilon}}^{\mu}\bar{\epsilon}^{n} \quad \text{(for proportional loading)}, \tag{8}$$

h_0 is given by the following expression:

$$h_0 = (1/3)[(n\bar{\sigma}/\bar{\epsilon}) + \beta\mu\bar{\sigma}], \tag{9}$$

where n = strain-hardening exponent (or the so-called n-value), μ = strain-rate sensitivity exponent, c = plastic modulus, and

$$\beta = \mathrm{d}(\ln \dot{\bar{\epsilon}})/\mathrm{d}\bar{\epsilon}$$

is called the strain-rate path coefficient which expresses the effect of strain-rate history. By making use of eqns (8) and (9), we can discuss about even the case where the material is of strain-rate dependence in a sense of natural time. Nevertheless, we concern here ourselves exclusively with the case of $\mu = 0$, i.e. n-th power hardening materials without viscous effect, because such materials are commercially most common except for a certain kind of particularly functionalized materials such as superplastic metals.

The algebraic fourth-order eqn (6) possesses real roots when

$$A = 0, \quad \text{or} \quad C \leqq -2\sqrt{AE} \tag{10}$$

holds, and at the instant where it first captures any real root a localized neck appears and the sheet breaks. Namely, the breakage condition is given as follows:

$$A = 0, \quad \text{or} \quad C = -2\sqrt{AE}. \tag{11}$$

The angle ψ between the 1-axis and the unit normal $\mathbf{g}$ to the localized necking band is given as follows:

$$\psi = 0 \quad (\text{for } A = 0), \quad \text{or} \quad \psi = \tan^{-1}(\sqrt[4]{A/E}). \tag{12}$$

As described in Part III, for proportional loading, the critical condition (11) can be solved analytically in a closed form with respect to the critical major strain $(\epsilon_1)_{cr}$ in terms of n and m or α. However, for arbitrarily nonproportional loading (or straining), it has to be solved numerically. Namely, the sheet element is deformed incrementally with appropriately small increment at every step of deformation, and the coefficients

$a_{11} \sim a_{33}$, and so forth, are evaluated to check the critical condition (11) or the change of the sign of A and $C + 2\sqrt{AE}$. The computer program for this purpose is made, which can also be used in a program for numerical analysis of plastic deformation of metal sheets as a subroutine to check when and where they break.

The numerical examples given below are mainly for the material of $n = 0.333$ and $\rho = 0.922$, which corresponds to a kind of aluminium-killed steel, and the theoretical FLD for proportional loadings with this value of ρ is confirmed to agree very well with the experiment. For simplicity and for a common aspect of scattering experimental data in breakage phenomenon, we assume the material to be isotropic, though sheet material usually shows planar and normal anisotropy (see, e.g. Part III).

For all numerical calculations here, the computer Facom M-200 at Nagoya University Computation Center is used.

3. NUMERICAL RESULTS AND DISCUSSIONS

3.1 *Nonproportional straining without unloading*

Figure 2 illustrates a lot of examples of limiting strain for various curved strain-paths. The increment of equivalent strain for one step of calculation is taken as $\overline{d\epsilon} = 0.005$. In the figure, the solid bold curve shows the FLD for proportional loadings (prop. FLD). The small letter 2 implies $\psi = 0$, i.e. the localized neck band is perpendicular to the 1-axis. From this figure, we find the following noticeable facts:

(1) A slight deviation of strain-path from a straight line (proportional loading) causes a fairly pronounced change in the limiting strain.

(2) An appropriately chosen curved strain-path gives a far greater limiting strain than that for the corresponding straight strain-path. Or, on the contrary, a badly chosen curved strain-path could cause a far smaller limiting strain.

The statement (1) seems to have to do with the fact that the experimental data of limiting strain are usually apt to scatter even for proportional loadings, because the control of strain-path is scarcely perfect (see Part III). On the other hand, the fact stated in (2) above can be applied effectively in the practical press-forming of metal sheets.

Next, let us consider the FLD for the case where the straight stress- or strain-path is abruptly changed to another straight one without unloading at the path change. When the stress-path is controlled, the strain-path after the path change is not straight and thus less severe change is caused with respect to strain-path than that in strain-path control case. But, of course, in both cases the directions of the stress- and strain-increments are abruptly changed at the path change. Therefore the calculation im-

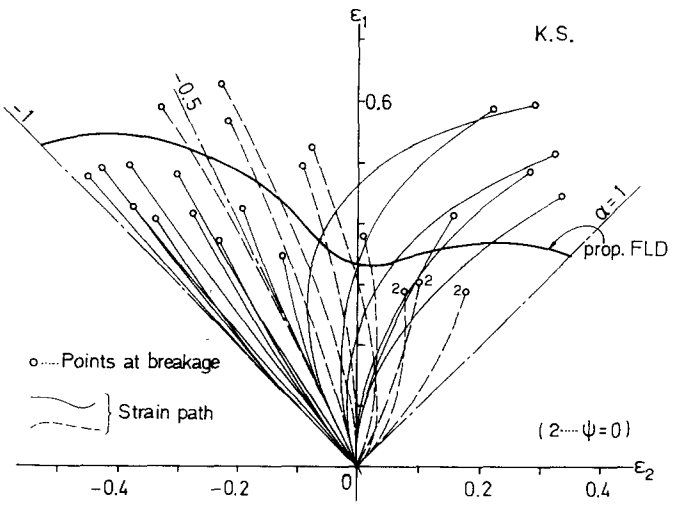

Fig. 2. Examples of limiting strain for various curved strain-paths.

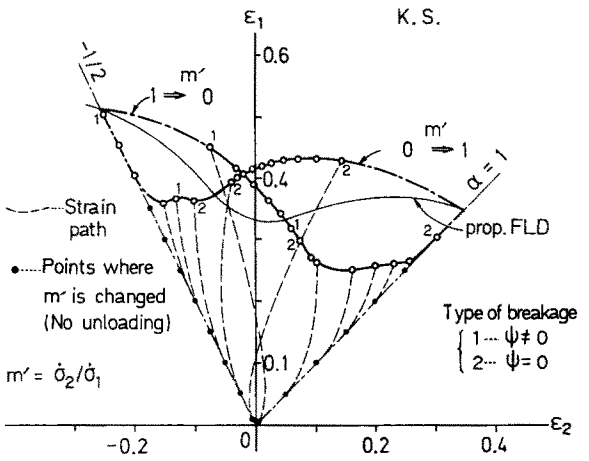

Fig. 3. Examples of FLD for stress-paths with an abrupt change in direction ($m' = 0 \rightarrow 1$ and $1 \rightarrow 0$; without unloading).

mediately after the path change should be performed with the finest of care. Here the increment of the equivalent strain at the steps after the path change is chosen as $\overline{d\epsilon} = 0.0001$ up to $\bar{\epsilon} = 0.02$ and then gradually increased to $\overline{d\epsilon} = 0.005$. All calculation is performed in double-precision.

Figures 3 and 4 illustrate the FLDs for the case of stress-path control. Figure 3 is for the case of $m' = 1 \rightarrow 0$ and $0 \rightarrow 1$, and Fig. 4 is for $m' = 1 \rightarrow -1$ and $-1 \rightarrow 1$. The curved broken lines in them show the strain-paths (prop. FLD is also inserted). The small letters 1 and 2 imply the direction of localized neck band by the angle $\psi \neq 0$ and $= 0$, respectively. From these figures we find the following interesting facts:

(1) When the degree of deformation along the first proportional loading does not exceed a certain amount, the limiting strain for the second stress-path increases beyond that for the corresponding proportional loading (i.e. beyond prop. FLD). However, when it does, the statement becomes converse.

(2) When the degree of deformation along the first proportional loading exceeds a certain amount greater than that in (1) above, the sheet breaks almost immediately after or at the instant of the path change. The statement (2) implies that an abrupt

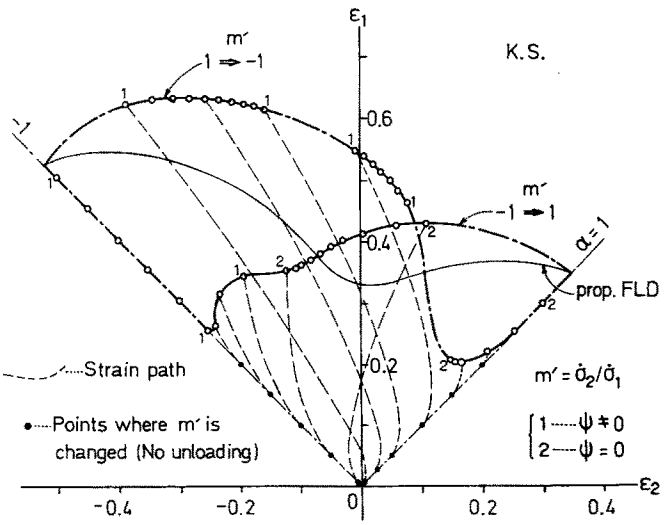

Fig. 4. Examples of FLD for stress-paths with an abrupt change in direction ($m' = 1 \rightarrow -1$ and $-1 \rightarrow 1$; without unloading).

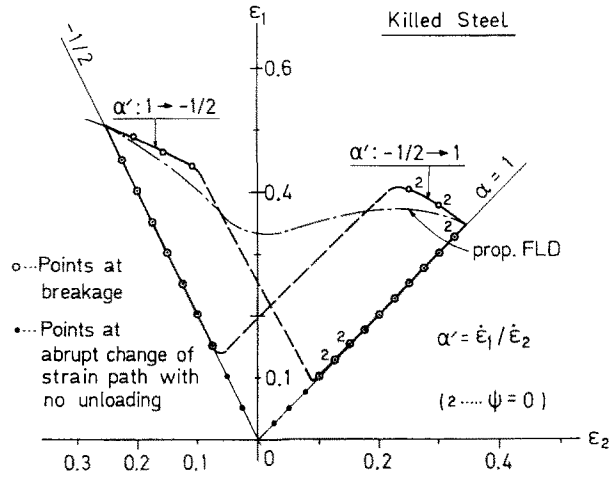

Fig. 5. Examples of FLD for strain-paths with an abrupt change in direction ($\alpha' = -0.5 \rightarrow 1$ and $1 \rightarrow -0.5$; without unloading).

change in stress-path may cause a catastrophic breakage of the sheet and thus should be avoided in press-working process.

Figure 5 illustrates the FLD for the case of strain-path control in which $\alpha' = 1 \rightarrow -0.5$ and $-0.5 \rightarrow 1$ are chosen. From this figure we find that the range of strain along the first proportional loading in which a catastrophic breakage of the sheet at the instant of the path change occurs is wider than that for the stress-control case. This is of course due to the fact that the degree of the state change is greater in the strain-control case than in the stress-control case.

The author once discussed about the effect of abrupt change of external condition on fracture of materials from a totally different point of view[8]. These results here give a kind of conclusion to the same subject from the viewpoint of bifurcation theory.

3.2 *Secondary FLD*

This is the FLD for the case of a proportional loading → unloading → the second proportional loading, i.e. FLD of prestrained metal sheets. This has its significance in press-forming of metal sheets which requires multistages of processes.

In the past, the secondary FLD has been mainly investigated by experiments especially in Japan[9]. And it is known that the secondary FLD for the case of $\alpha = -0.5$

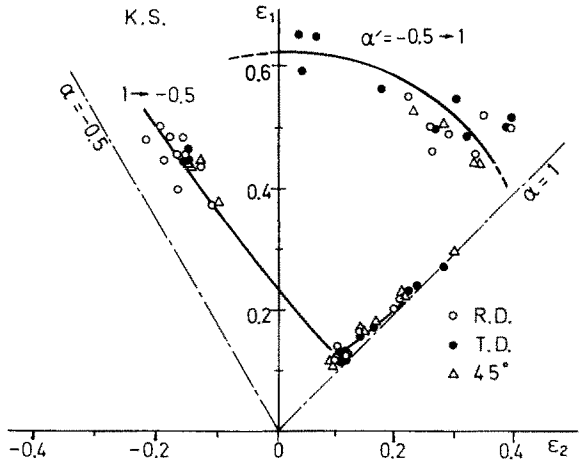

Fig. 6. Examples of the secondary FLD for the case of $\alpha' = -0.5 \rightleftarrows 1$ for a kind of aluminium-killed steel sheet (experiment).

(uniaxial tension) → unloading → $\alpha' = 1$ is the highest one and that for $\alpha = 1$ (equibiaxial tension) → unloading → $\alpha' = -0.5$ is the lowest one. They are called as the maximum and minimum forming limit diagrams, respectively. However, investigation on the secondary FLD is still very few. Other types of maximum and minimum FLDs could exist.

In the author's laboratory, we have also obtained experimental secondary FLDs of a few kinds of commercial metal sheets with respect to the case $\alpha' = -0.5 \rightleftarrows 1$. One of them is illustrated in Fig. 6 which is that of a kind of aluminium-killed steel plotted as the average curve of the three secondary FLDs for 0°, 45° and 90° to the rolling direction. From this figure, it is confirmed that the secondary FLD for $\alpha = -0.5$ → unloading → $\alpha' = 1$ is very high, and that for $\alpha = 1$ → unloading → $\alpha' = -0.5$ is very low. Particularly, in the latter, we find that deformation beyond a certain rather small strain along equibiaxial tensile strain-path exhausts the material ductility completely and the sheet breaks with no extension along the second strain-path of simple tension. This is rather similar to Figs. 3 and 5, though the latter figures are theoretical ones and, moreover, intermediate unloading is *not* allowed in them.

The constitutive equation (1) is based on the assumption that the subsequent yield surface in the deviatoric stress space is the Mises' super-sphere, except its portion of vertexed-cone due to vertex-hardening. This idealization is reliable as far as unloading is not involved during deformation. However, when unloading is given and reloading takes place along different stress- or strain-path from that of preloading, as in the secondary FLDs, it yields uncertainty; especially in strain-hardening characteristics in reloading process, which gives inconvenience in comparison of the theory with the corresponding experiments, because it is well known that the subsequent yield surface of the actual materials never takes that of Mises' type, and it changes its shape and its center moves with plastic deformation due to preloading. However, at present, the rule of subsequent hardening has not yet been established. Therefore, here we adopt the following rather simplified procedure which may be available only for the secondary FLDs. Namely, we introduce the following assumptions about the strain-hardening exponent $n^{(2)}$ and the half angle Θ_0 of the vertexed-cone along the second straight strain-path. First, for $n^{(2)}$, we use the following two formulas:

$$\text{(i)}\quad n^{(2)} = n, \tag{13}$$

$$\text{(ii)}\quad n^{(2)} = n^* = n[1 + k\theta^*\epsilon_a(\epsilon_{cr}^{(1)} - \epsilon_a)], \tag{14}$$

where $\epsilon_a = \bar{\epsilon}$ at the end of the first proportional loading, and $\epsilon_{cr}^{(1)}$ = the limiting equivalent strain when the sheet is deformed along the first proportional loading only. And θ^* denotes the angle which expresses the severity of the path-change from the first to the second strain-path, and is evaluated by the following expression which is based on the fact that the direction of deviatoric stress tensor in the deviatoric stress space is represented by its third-order invariant III_T:

$$\theta^* = \theta_2 - \theta_1, \tag{15}$$

$$\theta_i = \cos^{-1}(\overline{\mathrm{III}}_{\mathrm{T}(i)}), \tag{16}$$

$$\overline{\mathrm{III}}_\mathrm{T} = \mathrm{III}_\mathrm{T}/(\mathrm{III}_\mathrm{T})_{m=0}, \tag{17}$$

where $i = 1$ or 2 and it denotes the first or second proportional loading, respectively. As easily checked, $(\mathrm{III}_\mathrm{T})_{m=0} = (2/27)\sigma_1^3$. For example, the values of $\overline{\mathrm{III}}_\mathrm{T}$ defined by eqn (16) for a few cases are given as follows:

$$\overline{\mathrm{III}}_\mathrm{T} = \begin{cases} 1 \ldots \alpha = -0.5 & (m = 0), \\ 0 \ldots \alpha = -1 & (m = -1), \\ \quad\ = 0 & (m = 0.5), \\ -1 \ldots \alpha = 1 & (m = 1). \end{cases}$$

For example, for the case of $\alpha = -0.5 \rightarrow$ unloading $\rightarrow \alpha' = 1$, $\theta_1 = 0$ and $\theta_2 = \pi$ and thus $\theta^* = \pi$, and for the reversed case $\theta^* = -\pi$.

In eqn (14), k might be thought to be another material constant in general. Here, for simplicity and to avoid nuisance to add a new constant, we set it to be equal to unity. That is,

$$k = 1. \tag{18}$$

Of course, if needed in future, k may be treated as a material constant to fit the theoretical secondary FLDs more with the experimental data, if accuracy of the experiment is improved and the data are accumulated.

The derivation of eqn (14) is understood as follows: (i) $n^{(2)} = n$ for $\epsilon_a = 0$, because no unloading is involved. (ii) There is no reason to change the value of the hardening exponent and thus $n^{(2)} = n$ for $\epsilon_a = \epsilon_{cr}^{(1)}$, because the sheet breaks at $\bar{\epsilon} = \epsilon_a = \epsilon_{cr}^{(1)}$. (iii) $n^{(2)}$ will deviate more from n for greater severity of strain-path change.

The characteristics of strain-hardening for deformation along the second proportional loading is expressed by the following equation by use of $n^{(2)}$ in eqn (13) or (14):

$$\bar{\sigma} = c(\bar{\epsilon}_{(2)} + \epsilon_a)^{n^{(2)}}, \tag{19}$$

where $\bar{\epsilon}_{(2)}$ = equivalent strain along the second strain-path only.

Next, the angle Θ_0 for the second loading is formulated in the following two manners:

$$\text{(i)}\ \Theta_0 = (\pi/2) - \rho\bar{\epsilon}_{(2)}^2 = \Theta_1, \tag{20}$$

$$\text{(ii)}\ \Theta_0 = (\pi/2) - \rho(\bar{\epsilon}_{(2)} + \epsilon_a)^2 = \Theta_2, \tag{21}$$

where the value of ρ is chosen coincident with that of virgin material. (i) implies that the pointed vertex develops with second deformation with the same rate as that in the first deformation, whereas (ii) assumes that the vertex develops instantly at reyielding to the angle at the end of first loading and then evolves with deformation in a similar manner as along the first strain-path. For actual materials, the intermediate situation between (i) and (ii) will appear. As far as the value of the virgin material is used, these assumptions are unavoidable.

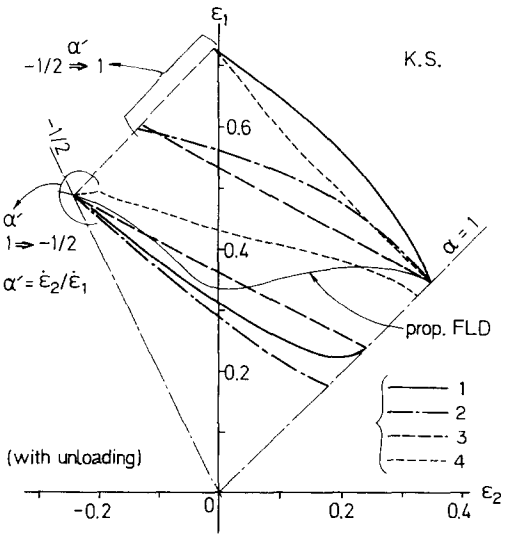

Fig. 7. Examples of theoretical secondary FLD for $\alpha' = -0.5 \rightleftarrows 1$.

Numerical examples of the secondary FLD are given below. In the figures, KS denotes the aluminium-killed steel sheet referred to previously.

Figure 7 illustrates the secondary FLD for the case of $\alpha' = 1 \rightleftarrows -0.5$ (prop. FLD is also inserted). The numbers of the curves designate $n^{(2)}$ and Θ_0 used in calculation according to the following:

$$1—n^{(2)} = n^*, \quad \Theta_0 = \Theta_1,$$
$$2—n^{(2)} = n^*, \quad \Theta_0 = \Theta_2,$$
$$3—n^{(2)} = n, \quad \Theta_0 = \Theta_2,$$
$$4—n^{(2)} = n, \quad \Theta_0 = \Theta_1.$$

The curves 3 are straight lines. Actually, when $n^{(2)} = n$ and $\Theta_0 = \Theta_2$ are adopted, the limiting equivalent strain $\epsilon_{cr}^{(2)}$ for the second strain-path is easily found to be

$$\epsilon_{cr}^{(2)} = \epsilon_{\max}^{(2)} - \epsilon_a, \tag{22}$$

where $\epsilon_{\max}^{(2)} = \epsilon_{cr}^{(2)}$ for $(\epsilon_a = 0)$ = the limiting equivalent strain of the virgin sheet when it is deformed along the same path as the second one. According to eqn (22), when $\epsilon_{cr}^{(1)}$ is greater than $\epsilon_{\max}^{(2)}$, the secondary FLD is coincident with the straight line which passes the point at which the virgin sheet deformed along the same proportional loading as the second path breaks, and the point corresponding to $\epsilon_a = \epsilon_{\max}^{(2)}$. In Fig. 7, this is the lower one of the straight lines numbered by 3. On the other hand, when $\epsilon_{cr}^{(1)}$ is less than $\epsilon_{\max}^{(2)}$, the secondary FLD is coincident with the straight line which passes the point corresponding to $\epsilon_{cr}^{(2)} = \epsilon_{\max}^{(2)} - \epsilon_{cr}^{(1)}$ on the second path starting from $\epsilon_a = \epsilon_{cr}^{(1)}$, and the breakage point of the virgin sheet deformed along the same path as the second one. In Fig. 7, this is the upper one of the straight lines numbered by 3.

The eqn (22) is coincident with the assumption used by Kikuma *et al.*[10] in calculation of the secondary FLDs. Here it is a logical result for the case of $n^{(2)} = n$ and $\Theta_0 = \Theta_2$.

All secondary FLDs in Fig. 7 agree at least qualitatively with those known so far. However, when we refer to the experimental result illustrated in Fig. 6, we find that the secondary FLDs numbered by 1 and 2 are better in a quantitative point of view.

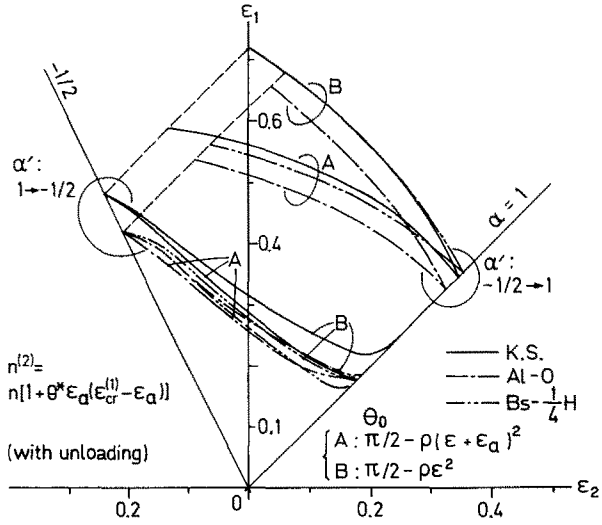

Fig. 8. Examples of theoretical secondary FLD for $\alpha' = -0.5 \rightleftarrows 1$ for three kinds of commercial metal sheets.

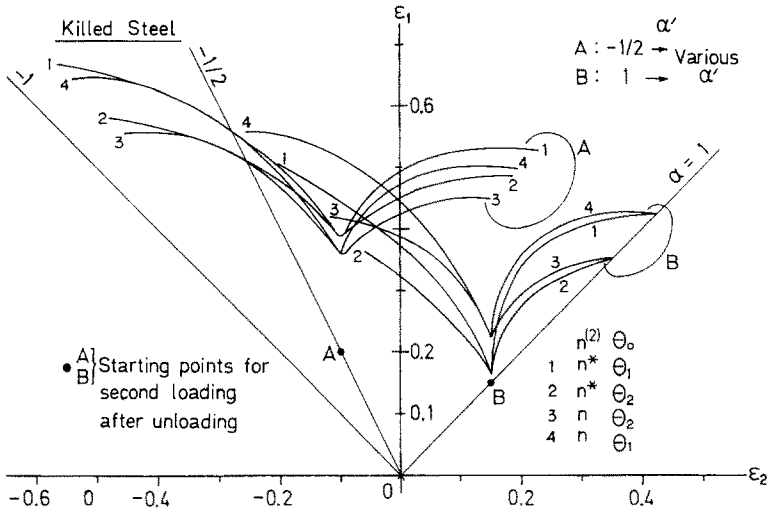

Fig. 9. Examples of theoretical secondary FLD for the case of $\alpha' = 1$ and $-0.5 \rightarrow$ arbitrary direction (KS).

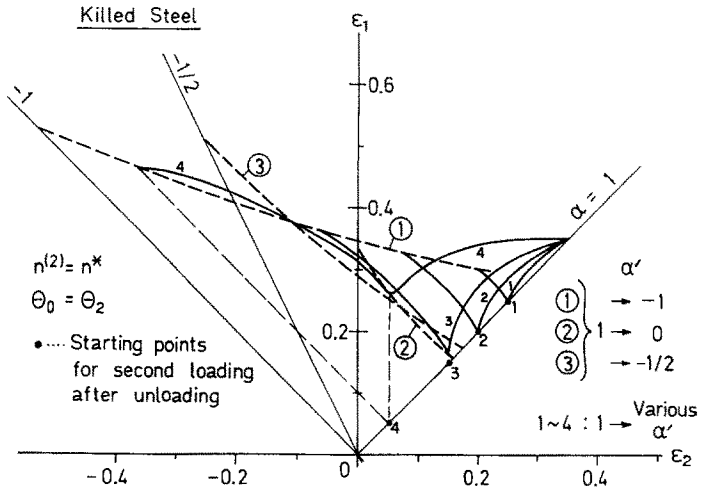

Fig. 10. Examples of theoretical secondary FLD for the case of $\alpha' = 1 \rightarrow$ arbitrary direction (KS).

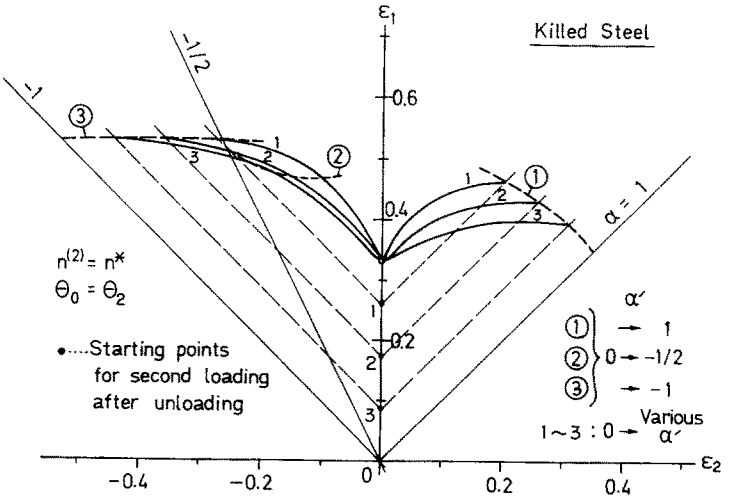

Fig. 11. Examples of theoretical secondary FLD for the case of $\alpha' = 0 \rightarrow$ arbitrary direction (KS).

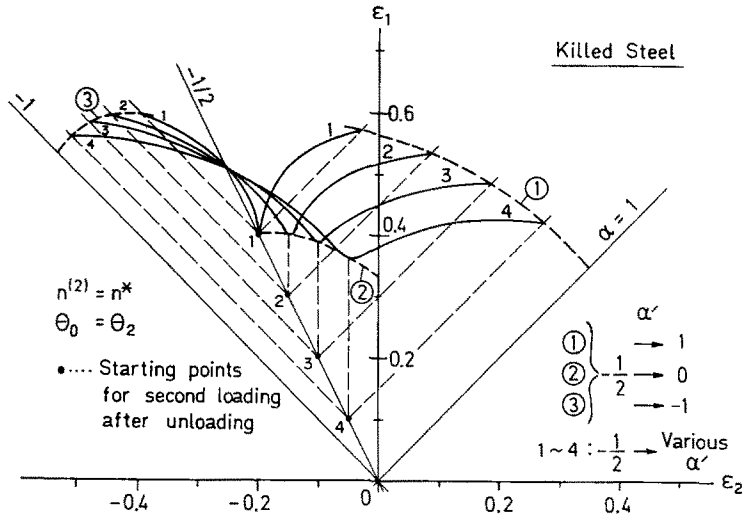

Fig. 12. Examples of theoretical secondary FLD for the case of $\alpha' = -0.5 \rightarrow$ arbitrary direction (KS).

That is to say, we can obtain the useful theoretical secondary FLDs in a practical sense by adopting $n^{(2)} = n^*$ and $\Theta_0 = \Theta_1$ or Θ_2.

Figure 8 illustrates the similar secondary FLDs of a soft aluminium (Al-0) and a quarter-hardness brass (Bs-$\frac{1}{4}$H), where $n^{(2)} = n^*$ and $\Theta_0 = \Theta_1$ or Θ_2 are used. The material constants are $n = 0.266$ and $\rho = 0.693$ for Al-0, and $n = 0.280$ and $\rho = 0.563$ for Bs-$\frac{1}{4}$H. In this figure, we see the similar feature of secondary FLDs for both metals as that for KS.

Figure 9 shows another type of illustration of the secondary FLD in which the sheet is deformed first along a straight strain-path, unloaded and then reloaded with various α' to get the FLD. In this figure, two points A and B are adopted as the starting state of the second loadings, where A and B are the points on the uniaxial tension ($\alpha = -0.5$) and on the equibiaxial tension ($\alpha = 1$). All the four types of choice of $n^{(2)}$ and Θ_0 are used, as in Fig. 7. The similar shapes of the secondary FLDs are seen for these four choices, which are also similar to those reported by Chu[5]. In a quanitative point of view, of course, they each show rather pronounced discrepancies.

Figures 10–15 ilustrate the examples of the secondary FLD which are obtained by straining the sheet along the second strain-paths with various α' following particular

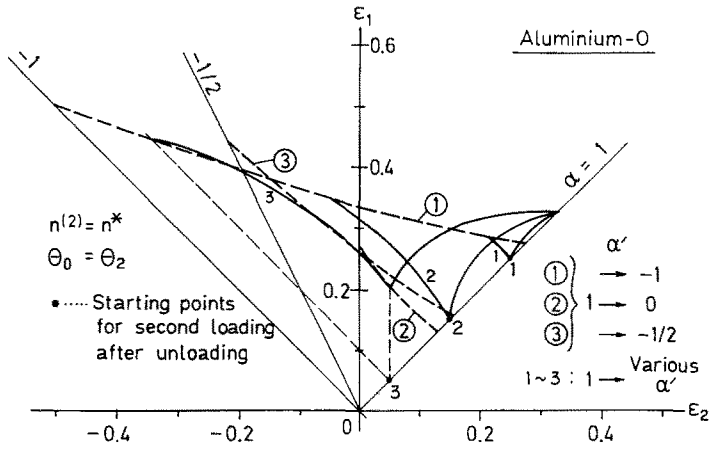

Fig. 13. Examples of theoretical secondary FLD for the case of $\alpha' = 1 \rightarrow$ arbitrary direction (Al-0).

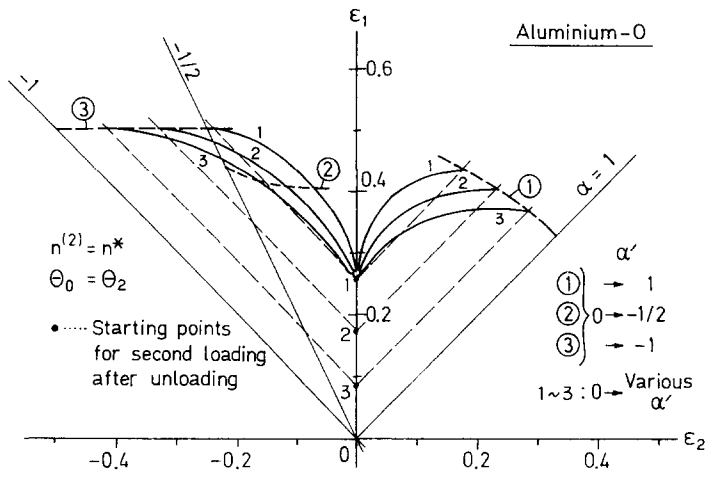

Fig. 14. Examples of theoretical secondary FLD for the case of $\alpha' = 0 \rightarrow$ arbitrary direction (Al-0).

proportional loadings. Figures 10–12 are for KS, and Figs. 13–15 for Al-0, where $n^{(2)} = n^*$ and $\Theta_0 = \Theta_2$ are adopted. The broken curves with encircled numbers in each figure are the secondary FLDs with respect to couples of α' inserted in the figure which follow the same method of illustration as those in Figs. 7 and 8, and thus appear as straight lines if $n^{(2)} = n$ and $\Theta_0 = \Theta_2$ are adopted.

In Fig. 10, we see that all the solid FLDs take their minimum points for second strain-path of $\alpha' = 0$. The FLDs from reloading points 1 and 2 involve some range of direction of reloading for which the sheet breaks almost immediately after or at the instant of reyielding. When we pay attention to the broken FLDs numbered by ② and ③, we find that a portion of ② locates lower than ③, which implies that the FLD for $\alpha' = 1 \rightarrow -0.5$ is *not* necessarily the minimum forming limit diagram. Note that the curve ③ is the same one as the lower one of the curves numbered by 2 in Fig. 7.

In Figs. 11 and 12, we also see that all the solid FLDs take their minimum points for second strain-path of $\alpha' = 0$. From a comparison of Fig. 11 and Fig. 12, we find that the secondary FLDs for $\alpha' = -0.5 \rightarrow 1$ and $\alpha' = 0 \rightarrow 1$ are the almost equivalent maximum forming limit diagrams. Note that the curve ① in Fig. 12 is the same one of the upper one of the curves numbered by 2 in Fig. 7.

Similar FLDs as those in Figs. 10–12 are obtained also for Al-0. Therefore it can be said that the difference in the secondary FLDs due to material properties appears qualitatively only.

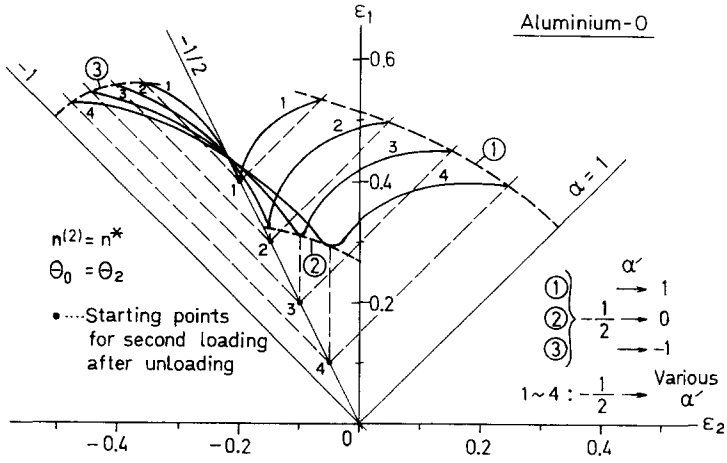

Fig. 15. Examples of theoretical secondary FLD for the case of $\alpha' = -0.5 \rightarrow$ arbitrary direction (Al-0).

5. CONCLUSIONS

The proposed constitutive equation is applied to prediction of the forming limit diagrams (FLDs) of metal sheets subjected to nonproportional loadings, in which the localized necking condition due to Stören and Rice is used as the breakage condition. Examples of limiting strain for arbitrarily curved strain-paths are given (Fig. 2), from which we find that a slight deviation of the strain-path from a straight line causes a rather pronounced change in the limiting strain, and that an appropriately chosen curved strain-path gives a far greater limiting strain than that for the corresponding proportional loading. The examples of FLDs are given for the case where the sheet is first deformed along a straight strain-path and then along another straight stress- or strain-path with an abrupt change of stress- or strain-path without intermediate unloading (Figs. 3–5). The sheet might break very often almost immediately after or at the instant of the stress- or strain-path change, in which the latter change gives more severe effect. The examples of the secondary FLD (i.e. FLD for the case where the sheet is deformed along a straight-path, unloaded and then reloaded along another straight strain-path) are also given by making use of appropriate assumptions on the strain-hardening exponent $n^{(2)}$ and Θ_0 for the second loading path, (Figs. 7–15). From a comparison of the theoretical curves with the experimental ones with respect to a kind of aluminium-killed steel sheet, it is concluded that such theoretical prediction of the secondary FLDs is very reliable for a practical use as well. The existence of the maximum and minimum forming limit diagrams is also verified. Finally, as for the limiting strains for nonproportional loadings and the secondary FLDs, much more accumulation of more reliable and accurate experimental data is inevitably required in the future.

REFERENCES

1. M. Gotoh, A class of plastic constitutive equations with vertex effect—I. General theory. *Int. J. Solids Structures*, **21**, 1101 (1985).
2. M. Gotoh, A class of plastic constitutive equations with vertex effect—II. Discussions on the simplest form. *Int. J. Solids Structures*, **21**, 1117 (1985).
3. M. Gotoh, A class of plastic constitutive equations with vertex effect—III. Applications to calculation of FLD of metal sheets. *Int. J. Solids Structures*, **21**, 1131 (1985).
4. S. Stören and J. R. Rice, Localized necking in thin sheets. *J. Mech. Phys. Solids* **23**, 42 (1975).
5. C.-C. Chu, An investigation of the strain-path dependence of the forming limit curve. *Int. J. Solids Structures* **18**, 205 (1982).
6. J. Christoffersen and J. W. Hutchinson, A class of phenomenological corner theory of plasticity. *J. Mech. Phys. Solids* **27**, 465 (1979).
7. Y. Ohashi, Effects of complicated deformation history on inelastic deformation behavior of metals. *Mem. Fac. Eng. Nagoya Univ.* **34**, 1–76 (1982).
8. M. Gotoh, The mathematical yield and/or fracture conditions of elastoplastic solids. *Arch. Mech.* **30**, 277 (1978).
9. Reports of Research Branch on Model Experiments (in Japanese), Japanese Research Group of Press-Forming of Thin Steel Sheets, Vol. 48 (1969).
10. T. Kikuma and K. Nakajima, Investigations on breakage of thin steel sheets. *Trans. Jpn Soc. Mech. Engrs., Ser.* A **45**, 1267 (1970).